Variation-Aware Layout and Design Optimization of Silicon Photonic Mach–Zehnder Interferometers

Zahra Ghanaatian, Amin Shafiee, and Mahdi Nikdast
Department of Electrical and Computer Engineering, Colorado State University, Fort Collins, CO 80523 USA

***Abstract*—We present an automated variation-aware layout and design optimization framework to enhance the robustness of silicon photonic Mach–Zehnder Interferometers (MZIs) under fabrication-process variations. Compared to conventional MZIs, the optimized MZIs show improved extinction ratio and optical-response uniformity by 18% and 90%, respectively.**

I. Introduction

Silicon photonic (SiPh) Mach–Zehnder Interferometers (MZIs) are one of the most crucial devices for the implementation of SiPh integrated circuits across different applications, including optical switches and filters, modulators, biosensors, and more recently 2×2 scalar multipliers for optical computing and photonic AI hardware accelerators [1]. Despite their wide range of applications, MZIs are sensitive to fabrication-process variations (FPVs). Small changes in the waveguide width and thickness due to FPVs cause significant phase errors and shifts in the MZI's optical frequency response. Moreover, any deviation from the ideal 50:50 splitting ratio in MZIs' directional couplers (DCs) leads to decreased extinction ratio, and hence increased crosstalk noise in the outputs [2]. These limitations have led to performance degradation upon scaling MZI-based SiPh integrated circuits [3].

In this paper, we propose an automated variation-aware layout and design optimization framework for MZIs under realistic and correlated FPVs in silicon-on-insulator (SOI) thickness and waveguide width. In particular, our optimization framework focuses on designing robust DCs and optimizing the layout and the design parameters (e.g., waveguide width) of MZIs' arms to minimize the phase-noise difference between the two arms. Leveraging realistic FPV maps, we show that our optimized MZIs can achieve a maximum extinction ratio of 38.3 dB with an average optical frequency-response shift of 2.9 nm with a standard deviation of 2.2 nm, showing high uniformity in the device response under FPVs.

II. MZI Layout and Design Optimization

The primary goal for variation-aware layout and design optimization in an MZI is to minimize the phase noise difference ($\Delta\phi_N$) between the two MZI's arms. Such a phase noise stems from the changes in the propagation constant (β) on each arm due to SOI thickness and waveguide width variations. Therefore, an optimization problem can be formulated as:

$$\begin{aligned} \min \quad & \Delta\phi_N = \left| L_1 \frac{\partial\beta_1}{\partial X} - L_2 \frac{\partial\beta_2}{\partial X} \right|, \\ \text{s.t.} \quad & \mathrm{f} \leq B, r_1, r_2 \leq R, g \leq G. \end{aligned} \tag{1}$$

Here, $\partial\beta_1$ and $\partial\beta_2$ show the changes in the propagation constant of arm1 and arm2, respectively. Also, X denotes the design parameter under variations which can be the waveguide width (w) or the SOI thickness (t). Note that in this paper we considered nonuniform variations across the MZI layout. f denotes the MZI's footprint which is bounded by B, a bounding box determining the maximum/desired area of the MZI. Moreover, r_1 (L_1) and r_2 (L_2) are the radius of the bends (length) in arm1 and arm2, respectively (see Fig. 1). R is the maximum radius of bends, and G and g are the maximum gap and the gap between the two arms, respectively. To address the optimization problem in (1), we first developed an automated tool that can take as inputs the desired area (i.e., B) and geometrical parameters of the MZI such as R and G, and the length difference between the two arms ($\Delta L = |L_1 - L_2|$)—determining the MZI's free-spectral range (FSR)—to generate an optimized MZI layout. The working principle of this layout-optimization tool focuses on modifying

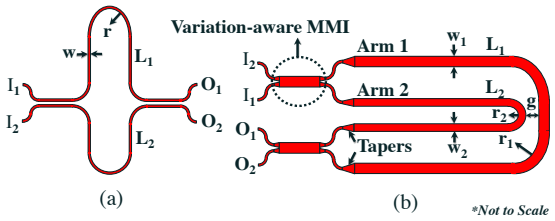

Fig. 1. Layout design of (a) conventional MZI and (b) optimized MZI.

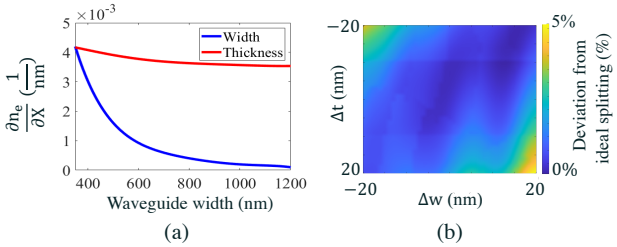

Fig. 2. (a) Rate of changes in the waveguide effective index (n_e) due to variations in the design parameter X. (b) The deviation of the designed MMI-based beam splitter's splitting ratio from nominal 50:50 under FPVs.

Date of publication: September 7, 2023. This work was accepted and will be presented at IEEE Photonics Conference (IPC) 2023.

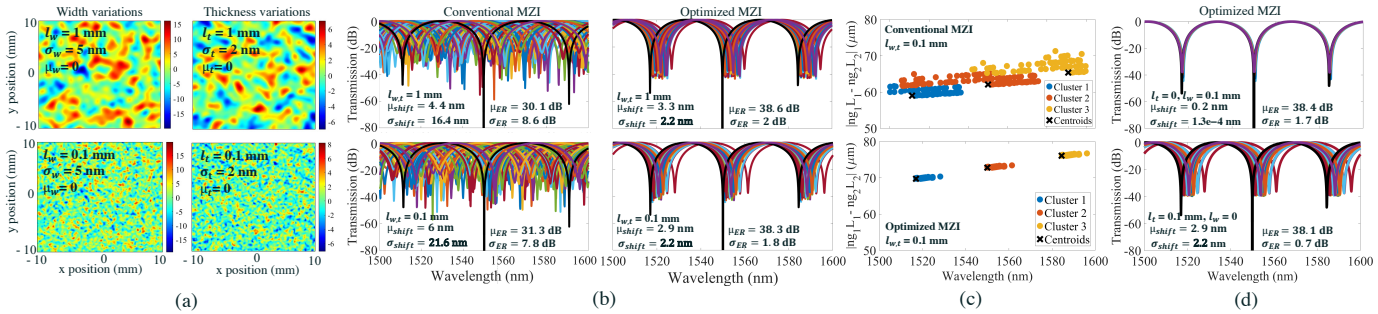

Fig. 3. (a) FPV maps. (b) Monte Carlo simulations of conventional and optimized MZIs under FPVs placed at different positions on the maps in (a). (c) K-means clustering of responses that belong to the same transmission group. (d) Monte Carlo simulations of optimized MZI under just width (top) and just thickness (bottom) variations.

the layout of a conventional MZI and pushing the arms as close as possible (see Fig. 1), to reduce $\Delta\phi_N$ by making them experience similar FPVs [3]. Leveraging an exhaustive search to minimize the gap between the arms (g), the optimum layout of the MZI and its corresponding arms' lengths can be obtained while satisfying the constraints in (1).

In addition to optimizing the MZI layout, MZI design parameters (e.g., waveguide width) can be optimized to further minimize $\Delta\phi_N$ (see (1)). To do so and reduce MZI's response sensitivity to X and hence minimizing $\Delta\phi_N$, we must enforce $\left(L_1\frac{\partial\beta_1}{\partial X} - L_2\frac{\partial\beta_2}{\partial X}\right) \rightarrow 0$. As a result, we can define a required design condition as [3], [4]:

$$\frac{L_1}{L_2} = \frac{\partial\beta_2/\partial X}{\partial\beta_1/\partial X}. \tag{2}$$

Changing the waveguide width can impact $\frac{\partial\beta}{\partial X}$ [5]. The rate of changes in the effective index ($\frac{\partial n_e}{\partial X}$)–note that $\beta = \frac{n_e\lambda}{2\pi}$—with t = 220 nm under FPVs and different waveguide widths (350–1200 nm) is shown in Fig. 2(a). Using these results and the obtained optimum MZI layout and arms' lengths (L_1 and L_2), we can use (2) to find the optimum waveguide widths on each arm. As it can be seen in Fig. 2(a), an increase in the waveguide width has a negligible effect on $\frac{\partial n_e}{\partial t}$ but considerably decreases $\frac{\partial n_e}{\partial w}$. Therefore, the resulting optimized MZIs will be more tolerant to width variations. Note that due to using different waveguide widths, waveguide tapers are required on each arm. The length of the tapers is designed to minimize optical mode distortion and higher-order mode excitation between waveguides of different widths (see Fig. 1(b)). Our analysis shows that a taper length of $\approx$1 μm is required for every 100 nm width difference.

Any variations in DCs in MZIs will impact their extinction ratio due to the changes in the ideal 50:50 splitting ratio. Instead of DCs, we designed and optimized multi-mode interference (MMI)-based beam splitters. To minimize the changes in the splitting ratio under FPVs, the length and width of the MMI-based beam splitter were optimized using a multi-variable simplex optimization method using Synopsys Rsoft tool. Electromagnetic simulations showed that the splitting ratio of the MMI-based beam splitter undergoes $\approx$ 5% deviation from nominal 50:50 splitting under aggressive $\pm$20 nm of width and thickness variations (see Fig. 2(b)).

III. Results and Discussions

Leveraging the proposed design optimization framework, we designed a variation-aware layout-optimized MZI with $W_1 = 1042$ nm, $W_2 = 1004$ nm, $L_1 = 301.5$ μm, $L_2 = 275.7$ μm, $r_1 = 10$ μm, $r_2 = 5$ μm, and $g = 5$ μm, as shown in Fig. 1(b). To statistically analyze the MZI's transmission spectrum under FPVs, we first created correlated variation maps with long-range ($l_{w,t} = 1$ mm) and short-range ($l_{w,t} = 0.1$ mm) correlated variations. Fig. 3(a) shows the maps with their mean (μ), standard deviation (σ), and correlation length ($l_{w,t}$). Fig. 3(b) shows the optical spectrum response of the conventional (with $W = 470$ nm, $L_1 = 301.5$ μm , $L_2 = 275.7$ μm, and $r = 5$ μm; see Fig. 1(a)) and the optimized MZIs when they are placed at 100 different random locations (same locations considered for the two MZIs) on the FPV maps while considering nonuniform variations. Results indicate that when $l_{w,t} = 1$ mm, the average optical response shift (μ_{shift}) from the nominal response at 1550 nm, and the corresponding standard deviation (σ_{shift}) is reduced from 4.4 nm and 16.4 nm in the conventional MZI to 3.3 nm and 2.2 nm in the optimized MZI, respectively. With $l_{w,t} = 0.1$ mm, these figures reduce from 6 nm and 21.6 nm to 2.9 nm and 2.2 nm. Note that to correctly calculate μ_{shift} and σ_{shift} related to the same optical response under FPVs—especially when the wavelength shift is larger than the FSR—we found optical responses belonging to the same transmission group based on $|n_{g_1}L_1 - n_{g_2}L_2| = \lambda^2/FSR$, where n_g is the group index [6]. Then, we used K-means clustering with centroids assigned to the nominal responses (shown in black in Fig. 3(b)) to cluster different responses which belong to the same transmission group (see Fig. 3(c)).

To better understand the source of wavelength shifts in our optimized MZI, Fig. 3(d) indicates the optimized MZI response under just width and just thickness FPVs with $l_{w,t} = 0.1$ mm (considered as an example). Note that under only width (thickness) variations, σ_{shift} and μ_{shift} are 1.3e$-$4 nm (2.2 nm) and 0.2 nm (2.9 nm), respectively. As discussed in Section II, this confirms that the main source of

wavelength shift in our optimized MZIs is the SOI-thickness variations. Moreover, the result of using optimized MMI-based beam splitters is reflected in the extinction ratio. As it can be seen in Figs. 3(b) and 3(d), the mean extinction ratio (μ_{ER}) related to the optimized MZI is increased by $\approx$ 8 dB compared to the conventional MZI using conventional DCs.

In summary, our proposed automated variation-aware layout and design optimization can help minimize wavelength shifts (and hence tuning power) and maximize extinction ratio in MZI-based photonic systems, including optical switches, interconnects, and coherent photonic neural networks.

ACKNOWLEDGMENT

This work was supported by the National Science Foundation (NSF) under grant number CNS-2046226 and CCF-2006788.

REFERENCES

[1] Y. Shen, N. C. Harris, S. Skirlo, M. Prabhu, T. Baehr-Jones, M. Hochberg, X. Sun, S. Zhao, H. Larochelle, D. Englund *et al.*, "Deep learning with coherent nanophotonic circuits," *Nature photonics*, vol. 11, no. 7, pp. 441–446, 2017.

[2] A. Shafiee, S. Banerjee, K. Chakrabarty, S. Pasricha, and M. Nikdast, "LoCI: An analysis of the impact of optical loss and crosstalk noise in integrated silicon-photonic neural networks," in *Proceedings of the Great Lakes Symposium on VLSI*, 2022, pp. 351–355.

[3] W. Bogaerts, Y. Xing, and U. Khan, "Layout-aware variability analysis, yield prediction, and optimization in photonic integrated circuits," *IEEE Journal of Selected Topics in Quantum Electronics*, vol. 25, no. 5, pp. 1–13, 2019.

[4] S. Dwivedi, H. D'heer, and W. Bogaerts, "Maximizing fabrication and thermal tolerances of all-silicon FIR wavelength filters," *IEEE Photonics Technology Letters*, vol. 27, no. 8, pp. 871–874, 2015.

[5] A. Mirza, A. Shafiee, S. Banerjee, K. Chakrabarty, S. Pasricha, and M. Nikdast, "Characterization and optimization of coherent MZI-based nanophotonic neural networks under fabrication non-uniformity," *IEEE Transactions on Nanotechnology*, vol. 21, pp. 763–771, 2022.

[6] L. Chrostowski, X. Wang, J. Flueckiger, Y. Wu, Y. Wang, and S. T. Fard, "Impact of fabrication non-uniformity on chip-scale silicon photonic integrated circuits," in *Optical Fiber Communication Conference*, 2014, pp. Th2A–37.